*Proc. R. Soc. Lond.* A **401**, 29–51 (1985)
*Printed in Great Britain*

# A two-dimensional imaging theory of surface discontinuities with the scanning acoustic microscope

By M. G. Somekh[1], H. L. Bertoni[2], G. A. D. Briggs[1] and N. J. Burton[3]†

[1] *Department of Metallurgy and Science of Materials, University of Oxford, Parks Road, Oxford OX1 3PH, U.K.*

[2] *Polytechnic Institute of New York, 333 Jay Street, Brooklyn, New York 11201, U.S.A.*

[3] *Department of Electrical and Electronic Engineering, University College, London WC1E 7JE, U.K.*

[Plate 1]

(*Communicated by Sir Peter Hirsch, F.R.S. – Received* 10 *September* 1984)

This paper discusses theoretical aspects of the $V(z)$ response of the scanning acoustic microscope (s.a.m.) when used to examine specimens with lateral discontinuities. The problem is introduced in terms of a simple ray model to establish a physical picture of the processes involved. An approximate Green function is then developed which enables use of a modified form of the Fourier optical formulations to calculate $V(z)$ for a cylindrical lens. These calculations explain two different types of contrast observed when imaging specimens in the reflection s.a.m., such as (i) the ability to image fine discontinuities and display them with enhanced contrast and an apparent width determined by the acoustic wavelength; and (ii) to give a quantitative account of the amplitude of periodic ripple often observed running parallel to cracks on acoustic micrographs. Both these types of contrast may be predicted by using the same model and arise naturally from variation of the reflection and transmission properties of the discontinuity, the relative value of these parameters determines which type of contrast predominates. At an interface between media with different elastic properties, the contrast is affected not only by the scattering properties of the boundary but also by the very fact that surface waves must propagate in media with different elastic properties. This effect alone can provide a powerful contrast mechanism which enables one to understand the light to dark contrast reversals often observed at grain boundaries in polycrystalline specimens at different values of defocus.

## 1. Introduction

When the reflection acoustic microscope is used to image solid objects such as integrated circuits and grain structure, the contrast between different parts of the object arises from the dependence of the output voltage, $V$, upon the defocus of

† Present address: V. G. Semicon Ltd, Imberhome Lane, East Grinstead, West Sussex RH19 1UB, U.K.

the specimen, $z$ (Quate *et al.* 1979). Different parts of the object will give different $V(z)$ dependences and will therefore show differing object brightness in the image. Often a dominant role in the determination of the contrast is played by the excitation of Rayleigh waves upon the surface of the specimen by the field incident from the couplant (usually water). The Rayleigh wave re-radiates sound into the couplant that returns to the transducer, which is added vectorially in the piezoelectric element to the acoustic field geometrically reflected from the object surface to produce the output voltage (Parmon & Bertoni 1979). The $V(z)$ in the region above the focus is different for each material or crystallographic orientation because the relative phase of the geometric and Rayleigh fields depends upon the Rayleigh velocity. When imaging at a given defocus, the output voltage and hence the image brightness for each portion of the object surface depends upon the value of $V(z)$ of the material present.

When the microscope is scanned over a region near to discontinuities in the object, such as a grain boundary, a crack or the edge of a deposited surface layer, the Rayleigh wave propagating away from the axis of the lens will be disturbed by the discontinuity. Broadly speaking, two types of image are observed in regions close to discontinuities, they may be described as either 'long-range' disturbances or 'short-range' disturbances. Long-range disturbances were first described by Yamanaka & Enomoto (1982), in which ripples were observed running parallel to a deep crack; the periodicity of these ripples was half the leaky Rayleigh wavelength, indicating that the acoustic microscope was detecting a standing wave pattern in the Rayleigh wave excitation. The interference was between the forward propagating leaky surface wave and that reflected from the crack. When the microscope is located directly over the discontinuity the propagation of leaky Rayleigh waves is disrupted so that the $V(z)$ may be strongly affected (Ilett *et al.* 1984). One result of this disruption is that surface-breaking cracks in an otherwise smooth surface may appear as dark areas against a light background, or as light areas against dark, depending upon the defocus. When the specimen is imaged at a defocus corresponding to a maximum of $V(z)$ for the continuous substrate a crack will generally appear dark: when imaging at a minimum it will usually appear bright. This short-range disturbance provides a powerful imaging mechanism in the s.a.m. because cracks with an opening displacement considerably smaller than the acoustic wavelength may be detected when they disturb the propagation of Rayleigh waves. For reasons that will become apparent later, we will designate contrast due to reflection at discontinuities as 'long-range' even when we are imaging close to the crack; in other words, long-range contrast is that contrast whose mechanism enables the presence of the crack to be observed a considerable distance away from the discontinuity.

To understand how discontinuities influence the image, the variations in the output voltage of the microscope when discontinuities are present in an otherwise uniform surface have been modelled. A simple approach to this problem has previously been taken for a cylindrical lens directly over a crack (Ilett *et al.* 1984). Calculations for the three-dimensional case of a spherical lens with a crack passing through its axis have been made by Cox & Addison (1984), by using a semi-numerical technique. In the present paper, however, we are concerned with the general case

when the lens is at an arbitrary position relative to the crack, and for this purpose we have again considered the two-dimensional case of a cylindrical lens. By using this model we have been able to provide a theory which explains both the long-range and the short-range imaging behaviour of the microscope. The specimen surface is depicted in figure 1, where the discontinuity lies in the plane $x = x_0$. For a grain boundary or a bonded interface between two different materials the elastic properties on either side of the discontinuity differ; for a crack, the material on either side may be the same. Both cracks and interface boundaries are treated here. The vertical position, $z$, of the surface is measured relative to the focal plane, negative values of $z$ corresponding to movement of the specimen towards the lens. To simplify the analysis the case of a cylindrical- or line-focus lens is treated. This renders the field problem two-dimensional and means that the leaky Rayleigh waves are only incident upon the discontinuity at normal incidence.

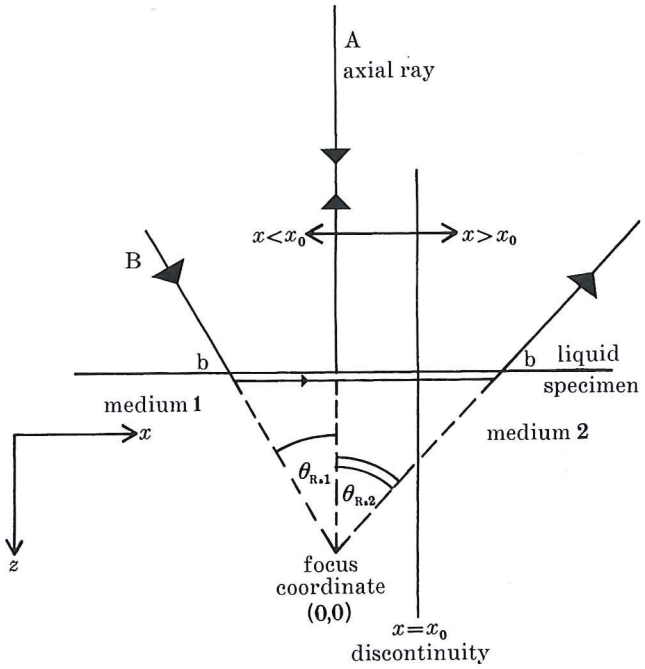


FIGURE 1. Schematic diagram of specimen, defining coordinate system and crack position.

The analysis uses Fourier optics to describe the propagation of the fields from the transducer to the object surface. To compute the field reflected by the object, we develop an approximate Green function integral that relates the field propagating back into the couplant at each point of the object surface, $x$, to the fields incident at all points of the surface, $x'$. The Green function for a surface with a discontinuity is obtained by generalizing the corresponding Green function for a smooth surface. This latter Green function is obtained by using the approach described by Saad *et al.* (1974), which separates the plane-wave reflection coefficient into a geometric and a leaky surface-wave part. The generalization of the smooth-surface Green

function to accommodate the presence of a discontinuity is most easily performed in the spatial $(x, x')$ domain. Subsequently the Green function is transformed to the spatial frequency domain, $(k_x, k'_x)$ so that Fourier optics can be used throughout this analysis. Here $k_x$ and $k'_x$ are the $x$ components of the wave vector in Fourier space of the reflected and incident fields respectively. The presence of scattering at the discontinuity means that the amplitude and phase at each value of $k_x$ depends on the amplitudes and relative phases of all the Fourier spectral components of the incident field, whose wavenumbers are designated by $k'_x$.

## 2. Application of simple ray theory

In this section we shall describe how a discontinuity can affect the contrast in the s.a.m. by perturbing the propagation of a Rayleigh wave along the surface of a specimen. We first describe the effect of a crack or grain boundary upon the contrast of the s.a.m. in terms of a simple ray model, which has the virtue of giving a very clear physical picture. To develop a more quantitative understanding of contrast from such discontinuities we shall find that we need to assess the proportion of the energy propagating along the specimen in the form of Rayleigh waves. This is discussed in §3.

It has long been established that the response of the scanning acoustic microscope for negative defocuses is dominated by excitation and re-radiation of leaky Rayleigh waves. A ray picture describing this $V(z)$ phenomenon considers that two principal rays make a significant contribution to the output response of the transducer. The first of these contributions is a result of the pencil of rays reflected directly from the specimen surface, shown as ray A of figure 1. The second significant contribution is depicted as ray B in figure 1, which results from rays incident from the liquid at or close to the angle $\theta_{\mathrm{Ra}} \approx \arcsin(V_{\mathrm{w}}/V_{\mathrm{Ra}})$ where $V_{\mathrm{w}}$ is the phase velocity of sound in water and $V_{\mathrm{Ra}}$ is the velocity of leaky Rayleigh waves on the solid. At this angle, waves incident from the water can couple efficiently into leaky Rayleigh waves, which propagate along the specimen surface shedding energy continuously back into the liquid at the angle $\theta_{\mathrm{Ra}}$. The leakage results in an attenuation, $\alpha_{\mathrm{Ra}}$, of the Rayleigh wave, additional to the attenuation, $\alpha_{\mathrm{D}}$, due to the intrinsic dissipation in the object material itself. With an implicit harmonic time dependence $\exp(-\mathrm{i}\omega t)$, in the absence of any exciting force on the surface the variation of the leaky Rayleigh wavefields along the surface has the form $\exp(\mathrm{i}k_{\mathrm{p}}x)$, where

$$k_{\mathrm{p}} = k_{\mathrm{Ra}} + \mathrm{i}(\alpha_{\mathrm{Ra}} + \alpha_{\mathrm{D}}) \tag{2.1}$$

and $k_{\mathrm{Ra}}$ is the real part of the wavenumber for leaky Rayleigh waves. The two ray contributions A and B add vectorially at the transducer so that the $V(z)$ response of the acoustic microscope depends upon the magnitude of the phasors produced by each acoustic beam component and the relative phase between them. As the specimen is defocused the relative phase between the two ray contributions changes so that the amplitude of the resultant output signal on the transducer oscillates with a periodicity in $z$ that is determined by $\theta_{\mathrm{Ra}}$, which is in turn related to the Rayleigh velocity.

A discontinuity in the surface is shown in figures 1 and 2. The first of these figures represents a crack placed within the spot on the surface illuminated by the incident field. This corresponds to the situation we described as a 'short-range' disturbance of the Rayleigh wave. Here, Rayleigh waves are excited from both points labelled b; these waves will hit the crack and be reflected with reflection coefficient $R$ and transmitted with a coefficient $T$. The crack scattering coefficients may depend upon the direction of the incident surface wave; we shall assume for cracks that $R$ and $T$ are the same for both directions of incidence. This assumption is not made, however, at interface boundaries. The theoretical determination of the values of $R$ and $T$ is a formidable problem (Achenbach *et al.* 1980), but we may nevertheless assume that every discontinuity may be characterized by these parameters. The values of $T$ and $R$ depend on the acoustic frequency because they are related to the ratio between the depth of the crack and the Rayleigh wavelength. Figure 2 represents the situation referred to earlier as 'long-range' disturbance; in this situation the surface wave is incident from one direction only and the transmission coefficient $T$ does not effect the final output of the transducer. To observe 'long-range' disturbances we would expect the crack to have a large reflection coefficient. In the short-range region of figure 1 we might expect that a small value of $T$ and $R$, corresponding to an absorptive crack (such as one scattering surface into bulk waves in the solid), would reduce the amplitude of the incoming Rayleigh wave so that the ripple normally associated with the $V(z)$ curve would be greatly reduced. These intuitive expectations will be compared with the more detailed wave model described in §5.

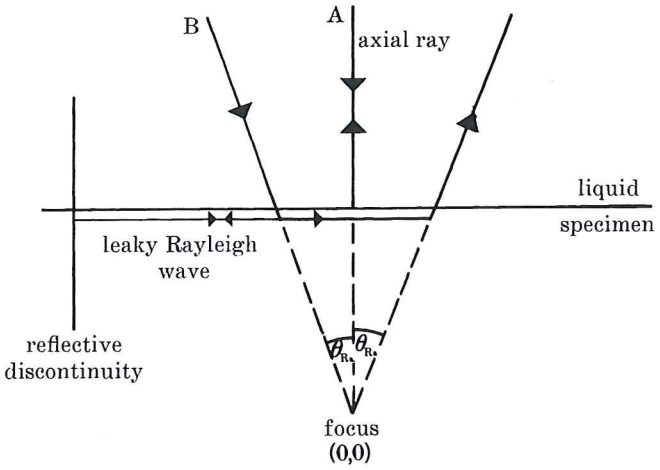


FIGURE 2. Ray diagram showing 'long-range' contrast mechanism.

Further effects in addition to scattering at a boundary arise when the specimen exhibits a discontinuous change in the Rayleigh wavenumber across the boundary. This may correspond to the situation in a composite material where two dissimilar materials are bonded together or a grain boundary where the different crystallographic orientations in each grain mean that the Rayleigh velocity differs across

the boundary. The change in the imaginary part of $k_p$ across the boundary means that energy is re-radiated more rapidly on one side of the boundary than the other. The change $k_{Ra}$, the real part of $k_p$, has more interesting consequences, however, because the angle of excitation of the Rayleigh wave will differ from the angle of re-radiation.

We shall now consider the effect of a velocity change across a boundary on the periodicity of the $V(z)$ ripple, by extending the simple analysis developed in Parmon & Bertoni (1979). We consider the situation where the boundary is well inside the illuminated area of the lens. We also assume that total transmission of the Rayleigh wave takes place at the boundary between two media, an assumption that would not normally be valid for a crack but which can be approximately true for a grain boundary. Because the angle of excitation, $\theta_{Ra1}$, in medium 1 differs from the corresponding angle in medium 2, $\theta_{Ra2}$ (the distance between the lens axis and point of excitation (and re-radiation)) is different in each material (see figure 1).

If a perfect reflector were placed at the focus of figure 1, rays A and B would return to the transducer in phase, because all rays must be in phase at the focus of an aberration-free lens. If we consider the specimen to be defocused towards the lens by a distance $z$, then the relative phase between the two rays may be computed as follows.

The advance in the phase of ray A is given by $2k_w z$, where $k_w$ is the wavenumber of the sound in water. The advance in the phase of ray B is

$$k_w z\left(\frac{1}{\cos\theta_{Ra1}}+\frac{1}{\cos\theta_{Ra2}}\right)-k_{Ra1}(z\tan\theta_{Ra1}+x_0)-k_{Ra2}(z\tan\theta_{Ra2}-x_0)+\psi, \quad (2.2)$$

where $x_0$ is the displacement of the boundary from the lens axis (see figure 4) and $\psi$ is a constant phase change associated with excitation and re-radiation of the Rayleigh wave. Because $k_{Ra} = k_w \sin\theta_{Ra}$, the relative phase between A and B, $\phi$, is

$$k_w z[(1-\cos\theta_{Ra1})+(1-\cos\theta_{Ra2})]+k_w x_0(\sin\theta_{Ra1}-\sin\theta_{Ra2})-\psi. \quad (2.3)$$

The periodicity in $V(z)$, $\Delta z$, is given by the change in $z$ necessary to produce a change in $\phi$ of $2\pi$:

$$\Delta z = \frac{2\pi}{k_w[2-(\cos\theta_{Ra1}+\cos\theta_{Ra2})]} = \frac{\lambda_w}{2-(\cos\theta_{Ra1}+\cos\theta_{Ra2})}. \quad (2.4)$$

When $\theta_{Ra1} = \theta_{Ra2}$, the expression is equivalent to that given for a continuous specimen by Parmon & Bertoni (1979), Atalar (1979) and Bertoni (1984). When the boundary is present the periodicity of the $V(z)$ ripple is intermediate between the periodicities of each region; to be precise the reciprocal of the periodicity is half the sum of the reciprocals of the periodicities corresponding to each region.

The foregoing expression applies only when the discontinuity lies between the points of excitation and re-radiation of Rayleigh waves. When $x_0$ lies outside this region the spacing between the minima, $\Delta z$, depends entirely upon the surface wave velocity of the material under the lens axis. The change in the location of the maxima and minima of the $V(z)$ curve as $x_0$ varies means that large changes in the output of the microscope can be expected at grain and interface boundaries. This effect depends primarily upon the change in the relative acoustic pathlengths

as the lens axis is moved relative to the discontinuity rather than on the scattering properties of the discontinuity itself. It will be shown in §5.2 that this additional mechanism for the contrast at an interface or grain boundary can be much more important than the scattering by the discontinuity. This distinguishes the two-media situation from the one-medium situation where the scattering at the crack is the sole determinant of the contrast.

To estimate the reflection and transmission coefficients of a Rayleigh wave at a boundary between two tightly bonded materials or a grain boundary, a transmission line model may be used to give a good approximation to the reflection and transmission coefficients, provided that the discontinuity is deep and smooth so that there is little scattering from the surface waves into bulk waves. The acoustic characteristic impedance of each medium is taken to be the density multiplied by the leaky Rayleigh wave velocity. This model yields $T_m = 1 + R_m$ where the letter m designates the medium and may be either 1 or 2. $T_m$ and $R_m$ are, respectively, the transmission and reflection coefficients from medium m (Li *et al.* 1977).

$$R_1 = -R_2 = \frac{\rho_2 k_{p1} - \rho_1 k_{p2}}{\rho_2 k_{p1} + \rho_1 k_{p2}}, \tag{2.5}$$

where $\rho_m$ and $k_{pm}$ are the density and leaky wave numbers of the two media. Because we are using a two-dimensional lens model throughout this work, we may treat a grain boundary as an interface between two different materials with Rayleigh wave velocities corresponding to the wave velocity in a direction perpendicular to the line of the interface. For a grain boundary, $\rho_1 = \rho_2$, so that

$$R_1 = \frac{k_{p1} - k_{p2}}{k_{p1} + k_{p2}} \approx \frac{k_{Ra1} - k_{Ra2}}{k_{Ra1} + k_{Ra2}}. \tag{2.6}$$

Calculations of the leaky Rayleigh wave velocities along various planes and directions in a fairly anisotropic material such as iron suggest that, for a typical grain boundary, the velocity difference between grains will be *ca.* 10% the reflection coefficient will be *ca.* 0.05 and a transmission coefficient of *ca.* 0.95. The small value of the reflection coefficient suggests that neglecting this parameter will not materially effect the conclusions of the ray calculation above; this is confirmed by the more detailed calculations presented in §5.2. The transmission line model of a grain boundary will be used with the more general wave analysis developed later in this paper. This simple ray approach will give an intuitive picture of the effects of lateral discontinuities, but to give a full account of the contrast a more quantitative assessment of the Rayleigh wave contribution must be made.

## 3. Separation of Rayleigh wave and derivation of the Green function

The simple ray approach discussed in §2 gives an intuitive picture of the effects of lateral discontinuities; the model we develop in this section enables one to make more precise predictions. In a model which recognizes the importance of the role of Rayleigh waves upon the microscope contrast it is necessary (at least implicitly)

to establish the coupling between the incident radiation from the liquid and hence the strength of the excited Rayleigh wave propagating along the solid–liquid interface.

### 3.1. *The field reflected at a uniform interface: calculation of the Rayleigh contribution*

In the absence of dissipation, $\alpha_D$ of (2.1) vanishes and $k_0$ at the zero of the plane wave reflection coefficient, $R_p$, is the complex conjugate of the pole at $k_p$. When $k_x$ is in the vicinity of $k_R$, the variation of $R_p(k_x)$ is dominated by the pole $k_p$ and zero $k_0$, and therefore is approximately given by the expression $(k_x-k_0)/(k_x-k_p)$. Similarly, when $k_x$ is near $-k_{Ra}$, the pole $-k_p$ and zero $-k_0$ dominate, so that $R(k_x)$ is approximated by the expression $(k_x+k_0)/(k_x+k_p)$. These two terms account for the phase change of $-2\pi$ that occurs in $R(k_x)$ as $\theta$ increases past $\theta_{Ra}$ (Atalar 1979). The foregoing two expressions may be factored out of $R(k_x)$. Let $R_0(k_x)$ be the ratio of $R(k_x)$ to the two expressions, so that

$$R_p(k_x) \equiv R_0(k_x)\left(\frac{k_x-k_0}{k_x-k_p}\frac{k_x+k_0}{k_x+k_p}\right) = R_0(k_x)\left(1+\frac{k_p^2-k_0^2}{k_x^2-k_p^2}\right). \tag{3.1}$$

The second term in the bracket accounts for the variation of $R_p(k_x)$ for $k_x$ in the neighbourhood of $\pm k_{Ra}$, because there the function of $R_0(k_x) \approx 1$. Away from $\pm k_{Ra}$, $k_x^2-k_p^2$ is large compared to $k_p^2-k_0^2$, so that $R_0(k_x) \approx R_p(k_x)$. In view of this behaviour of the terms in (3.1), $R_p(k_x)$ may be approximated as

$$R_p(k_x) \approx R_0(k_x)+(k_p^2-k_0^2)/(k_x^2-k_p^2). \tag{3.2}$$

The approximation (3.2) separates $R_p(k_x)$ into two parts. The first part, $R_0(k_x)$, describes all of the reflection properties of the surface except for those involving the Rayleigh wave, while the second describes the excitation and re-radiation of the leaky Rayleigh wave.

Let $p_i(x, z_0)$ be the pressure field incident on the surface located in the plane $z = z_0$, as shown in figure 1, and let $P_i(k_x, z_0)$ be its Fourier transform. Consistent with the foregoing separation of the reflection coefficient, we may separate the pressure $p_r(x, z_0)$ of the fields reflected into two parts:

$$p_r(x, z_0) = p_G(x, z_0)+p_L(x, z_0). \tag{3.3}$$

Here $p_G(x, z_0)$ is associated with $R_0(k_x)$ and $p_L(x, z_0)$ results from the Rayleigh wave. At a uniform surface, the Fourier transform of $p_r(x, z_0)$ is equal to the product of $P_i(k_x, z_0)$ and $R_p(k_x)$. By using the separation (3.2) of $R_p(k_x)$, we therefore have

$$p_G(x, z_0) = \frac{1}{2\pi}\int_{-\infty}^{\infty} R_0(k_x)\, P_i(k_x, z_0)\exp(ik_x x)\,dk_x \tag{3.4}$$

and

$$p_L(x, z_0) = \frac{1}{2\pi}\int_{-\infty}^{\infty} \frac{k_p^2-k_0^2}{k_x^2-k_p^2} P_i(k_x, z_0)\exp(ik_x x)\,dk_x. \tag{3.5}$$

An alternative form for $p_L(x, z_0)$ is derived by Bertoni (1984) by substituting for

$P_i(k_x, z_0)$ its representation in terms of the Fourier transform of $p_i(k_x, z_0)$ and changing the order of integration. This manipulation leads to

$$p_L(x, z_0) = \frac{1}{2\pi} \int_{-\infty}^{\infty} p_i(x', z_0) \left\{ \int_{-\infty}^{\infty} \frac{k_p^2 - k_0^2}{k_x^2 - k_p^2} \exp\left[ik_x(x-x')\right] dk_x \right\} dx'. \quad (3.6)$$

The integration over $k_x$ may be done by deforming the path of integration into the complex $k_x$ plane. For $x - x' > 0$, the path is deformed into the upper half-plane, capturing the pole at $k_p$. When $x - x' < 0$, deforming into the lower half-plane captures the pole at $-k_p$. By using the approximation

$$i(k_p^2 - k_0^2)/(2k_p) \approx -2\alpha_{Ra}, \quad (3.7)$$

valid when $\alpha_{Ra} \ll k_{Ra}$, the residues at the poles give

$$p_L(x, z_0) = -2\alpha_{Ra} \left\{ \int_{-\infty}^{x} p_i(x', z_0) \exp\left[ik_p(x-x')\right] dx' + \int_{x}^{\infty} p_i(x', z_0) \exp\left[-ik_p(x-x')\right] dx' \right\}. \quad (3.8)$$

Equation (3.8) is the Green integral for the leaky Rayleigh wave component of the reflected field. The first term in (3.8) represents the Rayleigh wave propagating in the positive $x$ direction, which is excited by the incident field at points to the left of the observation point. Similarly, the second term represents the leaky Rayleigh wave propagating in the negative $x$ direction and excited by the field incident to the right of the observation point.

### 3.2. *Fields reflected at a surface with a discontinuity*

In this section we generalize the results for a smooth surface to account in an approximate way for the presence of the discontinuity in figures 1 and 2. The primary effect of the discontinuity is to interfere with the lateral transfer of energy along the object surface. When present, the Rayleigh wave is the dominant mechanism by which lateral transfer of energy can take place. Anisotropic substrates may support other types of surface wave, such as pseudo-surface waves (Somekh *et al.* 1984), which transfer energy laterally; the present approach can probably be extended to these. The component $p_G(x, z_0)$ of the reflected field does include the weaker mechanism of lateral energy transfer by means of lateral waves, which are associated with the branch points of the reflection coefficient (Bertoni & Tamir 1973). The branch points are located at $\pm\omega/V_l$ and $\pm\omega/V_s$ in the complex $k_x$ plane, where $V_l$ and $V_s$ are longitudinal and shear velocities of the object. Neglecting scattering of the lateral waves by the discontinuity, and diffraction at the edge $(x_0, z_0)$, the field component $p_G(x, z_0)$ over each region of the object surface in figures 1 and 2 will be nearly the same as one would obtain for a uniform surface of identical properties. Thus if the medium is denoted by the subscript m = 1, 2, then

$$p_G(x, z_0) \approx \frac{1}{2\pi} \int_{-\infty}^{\infty} R_{0m}(k_x) P_i(k_x, z_0) \exp(ik_x x) dk_x. \quad (3.9)$$

In (3.9), the function $R_{01}(k_x)$ of medium 1 is used for $x < x_0$, while $R_{02}(k_x)$ is used for $x > x_0$. At grain and interface boundaries, $R_{01}(k_x)$ and $R_{02}(k_x)$ will be nearly

equal, so that an incident plane wave will reflect into a single plane wave with reflection coefficient $R_0(k_x)$.

The leaky Rayleigh wave excited to the left of the discontinuity and propagating towards it will be partly reflected with coefficient $R_1$ and partly transmitted with coefficient $T_1$. Provided that water loading is a small perturbation, these coefficients will be nearly the same as would be found for free surface Rayleigh waves in the absence of the couplant. Similarly, the leaky Rayleigh wave propagating towards the discontinuity from the right will be reflected and transmitted with coefficients $R_2$ and $T_2$. Some energy will be scattered directly into the water from the discontinuity. This energy is expected to be small compared with the reflected and transmitted energy, which is ultimately re-radiated into the water and is not considered. We also assume that the excitation and re-radiation factors of the Rayleigh waves are not affected by the proximity to the crack; i.e. we assume that the Green function is affected only by the reflection and absorption at the discontinuity.

In medium 1, the Rayleigh wave propagating in the positive $x$ direction is excited by fields incident to the left of the observation point. The re-radiated pressure of this wave is given by the first term in (3.8), where the parameters $\alpha_{\mathrm{Ra1}}$ and $k_{\mathrm{p1}}$ of medium 1 are used. The Rayleigh wave propagating in the negative $x$ direction will be composed of three parts. One part is due to excitation in medium 1 between the observation point and the discontinuity. Its radiated field is given by the second term in (3.8), with the upper limit replaced by $x_0$. The second part of the field propagating in the negative $x$ direction is produced by the Rayleigh wave incident on the discontinuity from the left and reflected by it. Because the incident wave is excited at all points $x < x_0$, the radiated pressure of this wave is given by

$$\exp\left[-\mathrm{i}k_{\mathrm{p1}}(x-x_0)\,R_1\right]\{-2\alpha_{\mathrm{Ra1}}\int_{-\infty}^{x_0} p_{\mathrm{i}}(x',z_0)\exp\left[\mathrm{i}k_{\mathrm{p1}}(x_0-x')\right]\mathrm{d}x'\}.$$

The third part of the wave propagating to the left in medium 1 is a result of the transmission of the wave incident on the discontinuity from medium 2, which is excited at all points $x > x_0$. Reciprocity requirements (Saad *et al.* 1974) require that the factor $\alpha_{\mathrm{Ra}}$ must be replaced by $\sqrt{(\alpha_{\mathrm{Ra1}}\,\alpha_{\mathrm{Ra2}})}$. The factor $\sqrt{(\alpha_{\mathrm{Ra2}})}$ arises from the excitation of the leaky wave on medium 2, while $\sqrt{(\alpha_{\mathrm{Ra1}})}$ describes the launching of the field in the water by the Rayleigh wave in medium 1. Thus the field of this last part is

$$\exp\left[-\mathrm{i}k_{\mathrm{p1}}(x-x_0)\right]T_2\left\{-2\sqrt{(\alpha_{\mathrm{Ra1}}\,\alpha_{\mathrm{Ra2}})}\int_{x_0}^{\infty} p_{\mathrm{i}}(x',z_0)\exp\left[-\mathrm{i}k_{\mathrm{p2}}(x_0-x')\right]\mathrm{d}x'\right\}. \tag{3.10}$$

The total radiated field for $x < x_0$ is therefore given by

$$\begin{aligned} p_{\mathrm{L}}(x,z_0) = -2\alpha_{\mathrm{Ra1}}\Bigg[\Bigg[&\int_{-\infty}^{x} p_{\mathrm{i}}(x',z_0)\exp\left[\mathrm{i}k_{\mathrm{p1}}(x-x')\right]\mathrm{d}x' \\ &+\int_{x}^{x_0} p_{\mathrm{i}}(x',z_0)\exp\left[\mathrm{i}k_{\mathrm{p1}}(x'-x)\right]\mathrm{d}x' \\ &+\exp\left[-\mathrm{i}k_{\mathrm{p1}}(x-x_0)\right]\left\{R_1\int_{-\infty}^{x_0} p_{\mathrm{i}}(x',z_0)\exp\left[\mathrm{i}k_{\mathrm{p1}}(x_0-x')\right]\mathrm{d}x'\right. \\ &\left.+\sqrt{\left(\frac{\alpha_{\mathrm{Ra2}}}{\alpha_{\mathrm{Ra1}}}\right)}\,T_2\int_{x_0}^{\infty} p_{\mathrm{i}}(x',z_0)\exp\left[-k_{\mathrm{p2}}(x_0-x')\right]\mathrm{d}x'\right\}\Bigg]\Bigg]. \end{aligned} \tag{3.11}$$

Similar arguments can be used to construct the field radiated in the region $x > x_0$. Thus, to the right of the discontinuity,

$$p_L(x,z_0) = -2\alpha_{Ra2}\Bigg[\Bigg[\int_{x_0}^{\infty} p_i(x',z_0)\exp[-ik_{p2}(x-x')]\,dx' + \int_{x_0}^{x} p_i(x',z_0)\exp[ik_{p2}(x-x')]\,dx' + \exp[ik_{p2}(x-x_0)]\Bigg\{R_2\int_{x_0}^{\infty} p_i(x',z_0)\exp[-ik_{p2}(x_0-x')]\,dx' + \sqrt{\left(\frac{\alpha_{Ra1}}{\alpha_{Ra2}}\right)}\,T_1\int_{-\infty}^{x_0} p_i(x',z_0)\exp[ik_{p1}(x_0-x')]\,dx'\Bigg\}\Bigg]. \tag{3.12}$$

Expression (3.8) together with (3.11) and (3.12) gives the complete reflected field at the object surface for any location $z_0$ of the surface, and any value of $x_0$.

### 3.3. *The Green function in the spatial frequency domain*

Equations (3.8), (3.11) and (3.12) can be viewed as relating $p_r(x,z_0)$ to $p_i(x',z_0)$ via a Green function $G(x,x')$ in the spatial domain. Alternatively, we can transform $G(x,x')$ to obtain a Green function $S(k_x,k_x')$ in the spatial frequency domain that relates the Fourier transform $P_r(k_x,z_0)$ of $p_r(x,z_0)$ to $P_i(k_x',z_0)$.

If we consider a unit incident wave of zero reference phase given by $\exp(ik_x'x')$ the spatial distribution upon reflection will be $\int_{-\infty}^{\infty} G(x,x')\exp(ik_x'x')\,dx'$. The angular spectrum corresponding to this spatial distribution will be given by the Fourier transform of this expression so that

$$S(k_x,k_x') = \frac{1}{2\pi}\int_{-\infty}^{\infty}\int_{-\infty}^{\infty} G(x,x')\exp(ik_x'x')\exp(-ik_x x)\,dx\,dx'. \tag{3.13}$$

This analysis gives a clear physical argument for the double Fourier transform relation that relates the Green function in one domain to the Green function in the other domain (Saad *et al.* 1974). It is the Green function $S(k_x,k_x')$ that is most convenient for computing $V(z)$ by using the Fourier optical techniques described in §4. This Green function allows the incident angular spectrum to be related to the reflected angular spectrum thus:

$$P_r(k_x,z_0) = \int_{-\infty}^{\infty} S(k_x,k_x')\,P_i(k_x',z_0)\,dk_x'. \tag{3.14}$$

Provided the correct allowance is made for the discontinuous change in the elastic constants across the boundary by convolution with the appropriate step function, lengthy but straightforward analysis for $S(k_x,k_x')$ leads to the expression

$$\begin{aligned} S(k_x,k_x') = {} & R_0\,\delta(k_x-k_x') \\ & + \frac{1}{2\pi}\Bigg\{2\sqrt{(\alpha_1\alpha_2)}\left[\frac{T_2'}{(k_x+k_{p1})(k_x'+k_{p2})}+\frac{T_1}{(k_x-k_{p2})(k_x'-k_{p1})}\right] \\ & - \frac{2\alpha_1}{k_x+k_{p1}}\left[\frac{1}{k_x'+k_{p1}}+\frac{R_1}{k_x'-k_{p1}}\right] - \frac{2\alpha_2}{k_x-k_{p2}}\left[\frac{1}{k_x'-k_{p2}}+\frac{R_2}{k_x'+k_{p2}}\right] \\ & + 4i\pi\delta(k_x'-k_x)\left[\frac{\alpha_1 k_{p1}}{(k_x)^2-(k_{p1})^2}+\frac{\alpha_2 k_{p2}}{(k_x')^2-(k_{p2})^2}\right] \\ & + \frac{4}{k_x'-k_x}\left[\frac{\alpha_1 k_{p1}}{(k_x')^2-(k_{p1})^2}-\frac{\alpha_2 k_{p2}}{(k_x')^2-(k_{p2})^2}\right]\Bigg\}. \end{aligned} \tag{3.15}$$

In (3.15) the first term represents the geometrical reflection whereas all the subsequent terms describe the behaviour of the excited Rayleigh waves. Equation (3.15) represents the most general case accounting for arbitrary values of the reflection and transmission coefficients and also allowing for different media either side of the boundary. If $T_1 = T_2 = 1$ and $R_1 = R_2 = 0$ and $k_{p1} = k_{p2}$ this expression reduces to the form of (3.2), the reflectance function from a single material in the absence of a discontinuity. A crack in a single material is represented by $k_{p1} = k_{p2}$.

A consequence of the model used is that the effects of the crack on the term representing the geometrical reflection are completely neglected, so that in some cases the total spectral power reflected can be greater than unity. The errors arising from this approximation in practice are believed to have only a small effect on the contrast in the microscope, but they remain to be evaluated. Although the method of analysis does not depend on a perturbation approach, (3.15) has the form of a perturbation solution in that the solution for a material with a crack is expressed as the specular reflection from a perfect specimen with additional non-specular terms caused by the presence of the crack. It would be reasonable to expect therefore that (3.15) is most accurate for comparatively weakly scattering discontinuities.

## 4. Calculation of $V(z)$

In this section we shall derive expressions for $V(z)$ for a cylindrical lens that are very similar in form to those given by Sheppard & Wilson (1981). First, $V(z)$ for a perfect defect-free substrate will be derived so that the stages necessary in the analysis are clear. An expression for $V(z)$ in the presence of defects will then be derived; in this expression the scattering function $S(k_x, k'_x)$ will fulfil the same role as the reflectance function in a perfect substrate.

### 4.1. *$V(z)$ for a 'defect-free' substrate*

Let the lens produce an angular spectrum $L_1(k_x)$ at the focus. The actual form of this angular spectrum will depend on the geometry and construction of the lens and transducer but may be regarded as a measurable parameter of the system. On propagation to the specimen the angular spectrum will be modified to $L_1(k_x) \exp(ik_z x)$ where $k_z = \sqrt{(k^2 - k_x^2)}$. Reflection from a perfect surface involves no change in the $x$ component of the wavenumber so that on reflection this will still be $k_x$.

This spectrum then propagates back to the focus so that the returning angular spectrum at focus is $R_p(k_x) L_1(k_x) \exp(2ik_z z)$. We now define a further empirical lens parameter $L_2(k_x)$, which gives the voltage response of the transducer to a plane wave of unit amplitude at the focus. $L_2(k_x)$ is thus the sensitivity function of the lens. We may now write:

$$V(z) = \int_{-\infty}^{\infty} L(k_x) R_p(k_x) \exp(2ik_z z)\, dk_x, \tag{4.1}$$

where $L(k_x)$ is the product of the functions $L_1$ and $L_2$ and the integration limits are unbounded because the aperture of the lens is bounded.

### 4.2. *V(z) for a specimen with a lateral discontinuity*

When the specimen contains lateral discontinuities, a plane wave incident at one incident angle $k'_x$ will be scattered into a spectrum of plane waves given by the scattering function $S(k_x, k'_x)$. Because the incident waves with a $k'_x$ component of wavenumber are scattered into plane waves propagating with different $k_x$, we must be careful to distinguish between the $x$ component of the wavevectors of incident and scattered waves. With a specimen without discontinuities this distinction is unnecessary because they are the same. As for a perfect reflector the angular spectrum at the focus will be $L_1(k'_x)$, so that the spectrum incident upon the surface is $L_1(k'_x)\exp(\mathrm{i}k'_z z)$. We now move our coordinate system so that the plane $x = 0$ corresponds to the line of the discontinuity ($x = x_0$) rather than the axis of the lens as implicitly assumed previously. This is done so that the scattering matrix is calculated once only for an incident wave of unit amplitude and zero phase; the effect of moving the crack is incorporated in the phase change introduced when the coordinate system is changed. The incident angular spectrum in the modified coordinate system is $L_1(k'_x)\exp[\mathrm{i}(k'_z z + k'_x x_0)]$. Because the reflected spectrum is now expressed in a coordinate system in which the crack position is the origin, the reflected angular spectrum may be obtained by direct application of the scattering function; the spectrum is thus $S(k_x, k'_x)\,L_1(k'_x)\exp[\mathrm{i}(k'_z z + k'_x x_0)]$. To account for the back-propagating spectrum, each component of the returning spectrum is once again referred to the original coordinate system and allowed to propagate back to the focus, so that the amplitude and phase of each wave is

$$\exp[\mathrm{i}(k_z z - k_x x_0)]\,S(k_x, k'_x)\,L_1(k'_x)\exp[\mathrm{i}(k'_z z + k'_x x_0)].$$

The returning angular spectrum at the focus may therefore be evaluated from the integral

$$\int_{-\infty}^{\infty} \exp[\mathrm{i}(k_z z - k_x x_0)]\,S(k_x, k'_x)\,L_1(k'_x)\exp[\mathrm{i}(k'_z z + k'_x x_0)]\,\mathrm{d}k'_x.$$

The $V(z)$ output response of the system is thus

$$V(z) = \int_{-\infty}^{\infty}\int_{-\infty}^{\infty} \exp[\mathrm{i}(k_z z + k'_z z)]\,L_1(k'_x)\,L_2(k_x)\,S(k_x, k'_x) \times \exp[\mathrm{i}(k'_x x_0 - k_x x_0)]\,\mathrm{d}k'_x\,\mathrm{d}k_x, \quad (4.2)$$

where $k_z$ and $k'_z$ must be expressed in terms of $k_x$ and $k'_x$ respectively. If $S(k_x, k'_x)$ is replaced by $R(k_x)\,\delta(k_x - k'_x)$, then (4.2) reduces to the form of (4.1).

## 5. Calculated results

### 5.1. *Results from a crack in a single medium*

The scattering function for a crack was calculated from (3.15) for various values of $T$ and $R$ and substituted into (4.2) so that the $V(z)$ response of the cylindrical lens could be calculated for a crack with various reflection and transmission properties. Figure 3 shows the $V(z)$ response calculated for aluminium by setting

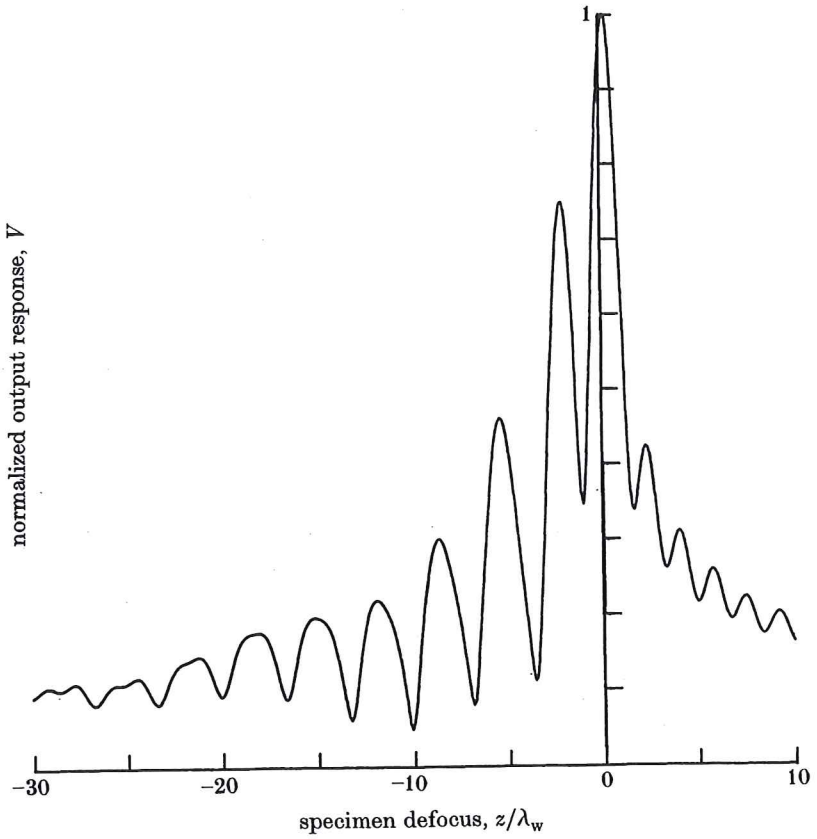


FIGURE 3. $V(z)$ obtained for a 'perfect' specimen with unity crack transmission coefficient and zero reflection coefficient. The elastic constants correspond to those of aluminium, longitudinal velocity = 6331 m $s^{-1}$, shear velocity = 3109 m $s^{-1}$, Rayleigh velocity = 2903 m $s^{-1}$, density = 2695 kg $m^{-3}$; wave velocity in water at 60 °C = 1551 m $s^{-1}$ with density = $10^3$ kg $m^{-3}$.

$T = 1$ and $R = 0$; that is, in the absence of any discontinuity. Figure 4 shows the calculated $V(z)$ when $T = 0.5$ and $R = 0$ (this corresponds to an absorptive discontinuity) for different displacements between the crack and the axis of the acoustic lens. This series of $V(z)$ curves shows the effect of moving the lens axis away from the crack position. A calculation for the situation where the crack is displaced from the lens axis by *ca.* $10\lambda_w$ (where $\lambda_w$ is the acoustic wavelength in water) shows that the $V(z)$ response is very similar to that of the material in the absence of the discontinuity. Linear discontinuities of low reflectance are therefore responsible for the 'short-range' contrast referred to earlier. The solid curve in figure 5 shows a $V(x)$ plot taken at a defocus of $-2\lambda_w$. A $V(x)$ curve is a plot of output voltage against the displacement of the lens position relative to the crack, and corresponds to the output of the line scan of the acoustic microscope. This figure shows that the contrast due to this discontinuity is very small at a distance more than $3\lambda_w$ away from the crack, thereby confirming our description of short-range contrast. As the defocus is increased, the apparent width of the crack

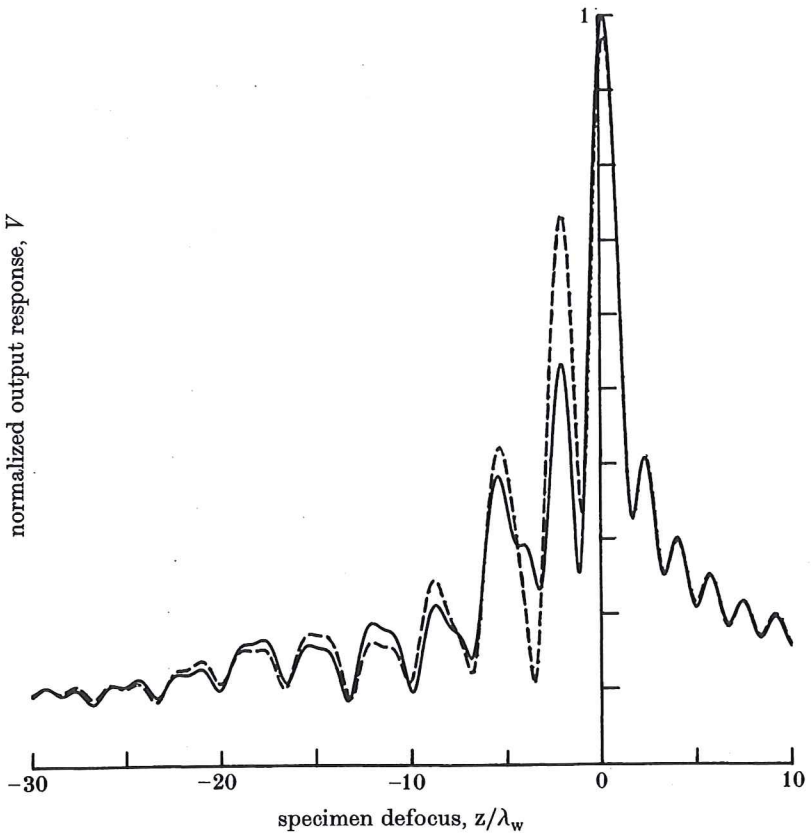


FIGURE 4. $V(z)$ curves obtained from aluminium with an absorptive, non-reflecting crack with $T = 0.5$ and $R = 0$. Solid curve represents axial crack. Broken curve represents crack displaced by $4\lambda_w$ from the lens axis.

(defined as the distance between the points at which the contrast falls to half its maximum value) corresponds more closely to the value $2z \tan\theta_{Ra}$, which is the distance between excitation and re-radiation of Rayleigh waves as predicted by ray theory. For values of defocus greater than about $5\lambda_w$ this value gives a reasonable, although not excellent, estimate of the apparent crack width. Measurements taken from a similar $V(x)$ curve taken at focus indicate first that the contrast between the crack and the rest of the surface is small, and secondly that the width of the crack appears to be *ca.* $1.5\lambda_w$, by using the above criterion. The profile of the image of the crack is such that the apparent width is strongly dependent upon the exact criterion one uses. Nevertheless, at focus the apparent width of a non-reflective discontinuity appears to be determined by the diffraction-limited spot size in water. This confirms the comments of Quate (1980) on the apparent width of grain boundaries. For a two-dimensional lens the distance between excitation and re-radiation of Rayleigh waves, rather than the spot size, seems to determine the apparent width of the discontinuities. At focus this value is indistinguishable from the spot size, because at focus Rayleigh waves may be

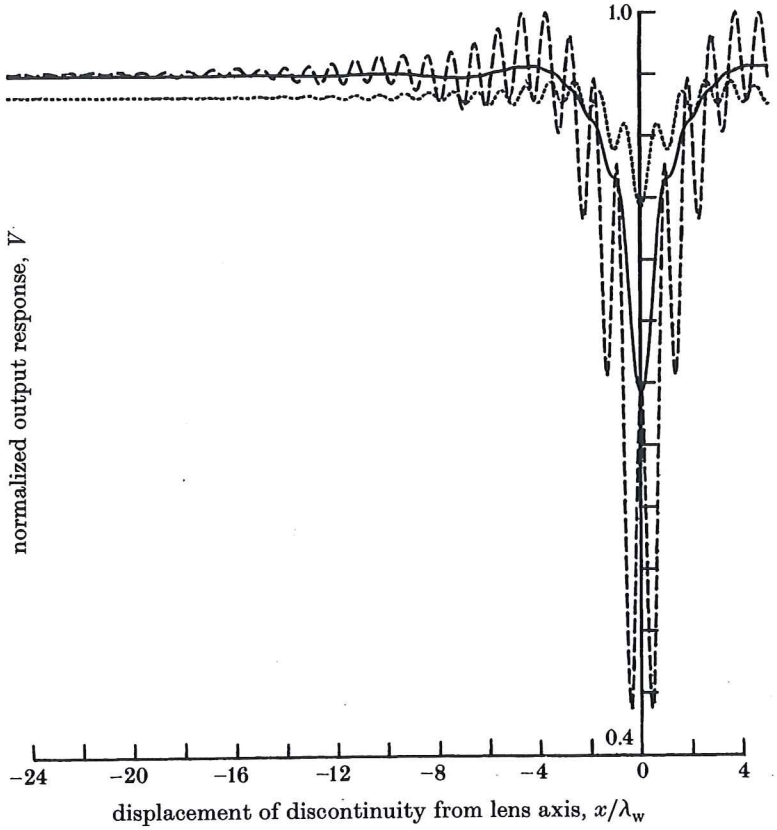


FIGURE 5. $V(x)$ curves obtained at a specimen defocus of $-2\lambda_w$. Solid curve represents specimen with the same parameters as in figure 4. Broken curve represents aluminium with reflective discontinuity ($T = 0, R = 0.5$). Dotted curve represents hybrid discontinuity using the same data as shown in figure 8*a*.

regarded as excited throughout the extent of the focused beam because a particular spatial position will not correspond to a particular incident angle. When the beam is defocused, diffraction effects will be less important and the distance between excitation and re-radiation will be adequately predicted by ray theory. The situation for a two-dimensional lens when defocused will be rather different from that of a spherical imaging lens because in the spherical case the annulus of the excited surface waves will be self-focusing. This was discussed qualitatively by Smith *et al.* (1983), where the authors concluded that this self-focusing effect would mean that the apparent width would only slowly increase with defocus.

We will now look at the calculated microscope response when the properties of the crack are reversed, i.e. when $T = 0$ and $R = 0.5$. Figure 6 shows a series of values of $V(z)$ calculated from these crack parameters. When the crack is on the lens axis, $V(z)$ is exactly the same as that shown in figure 4 (solid curve) for an absorptive crack. This is because the ray paths in each are equivalent, so that the ray reflected from the crack follows precisely the same path and has the same magnitude as the

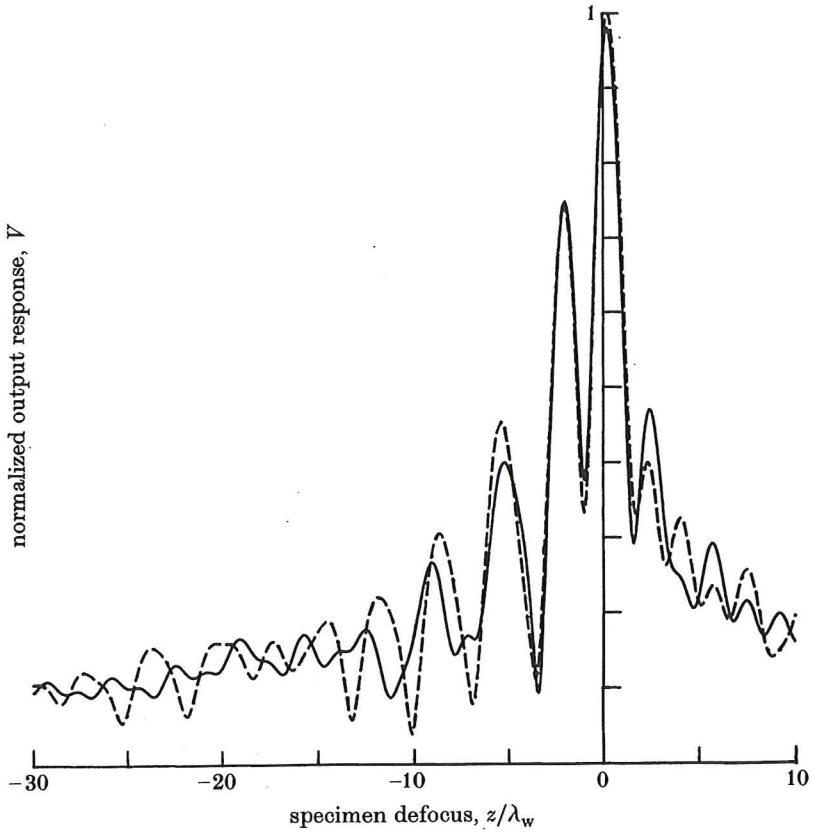


FIGURE 6. $V(z)$ curves obtained from aluminium with reflective discontinuity ($T = 0$, $R = 0.5$). Solid curve represents crack displaced by $4\lambda_w$ from lens axis. Broken curve represents crack displaced by $10\lambda_w$ from lens axis.

ray transmitted through the crack which gave rise to the solid curve in figure 4. As the crack is moved from the central position, the $V(z)$ curves of figure 6 become very different from those of figure 4. The most interesting feature is that $V(z)$ is severely perturbed in the positive $z$ region, that is, when the specimen is placed below the focal plane. The diagram of figure 7 illustrates why this may occur. The principal surface waves excited on the specimen surface when the specimen is below the focal plane travel away from the lens axis and thus do not contribute significantly to the $V(z)$ response of the acoustic lens. If, however, these rays are reflected from the discontinuity they may return to the lens along their original path, thus significantly affecting the microscope response. This prediction provides a simple experimental test of whether a linear discontinuity is reflective. The broken curve of figure 5 shows a $V(x)$ curve calculated for a defocus of $2\lambda_w$. One can see immediately that here the contrast extends a very considerable distance. There is ripple with a periodic variation of half the Rayleigh wavelength which is responsible for the long-range contrast, and this may be thought of as superimposed upon a varying baseline which represents short-range contrast localized within a

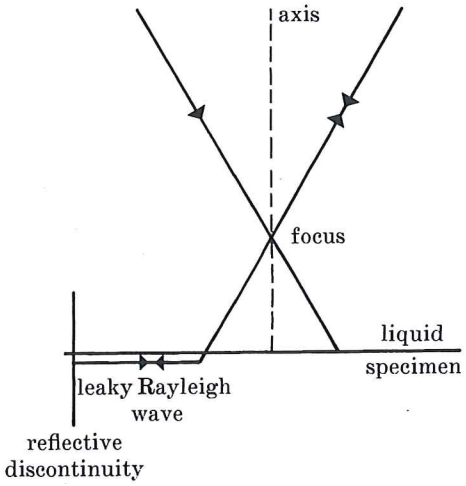


FIGURE 7. Ray diagram explaining why the $V(z)$ curve is perturbed in the positive $z$ region in the presence of a reflective discontinuity.

few wavelengths of the crack. The reflective discontinuity thus exhibits both long- and short-range contrast mechanisms. As one moves away from the crack the localized variation in the contrast dies out and one is left with just the periodic ripple of the type observed by Yamanaka & Enomoto (1982), whose amplitude decays exponentially according to $\exp(-2\alpha_{\mathrm{Ra}} x_0)$. The $V(x)$ curves bring out the distinction between reflective cracks, which affect the contrast in the acoustic images over a distance of ten or more Rayleigh wavelengths, and absorptive discontinuities whose effects on the contrast are much more localized. The strength of the model presented here is twofold: first, it is able to explain the contrast due to a discontinuity at any point quantitatively, and secondly, the same model is applicable both near and far from the discontinuity.

Angel & Achenbach (1984) have recently calculated the amplitude and phase of the reflection and transmission coefficients of Rayleigh waves incident upon a crack at an arbitrary angle of incidence. The values of the reflection and transmission coefficients were calculated for a range of crack depths. If we assume that these scattering coefficients are little affected by the liquid loading then the values for normal incidence may be substituted into (4.2) to compute either $V(z)$ or $V(x)$ curves. Cox & Addison (1984) have similarly computed $V(z)$ in their model of a spherical lens with a crack on the axis by using these coefficients. Figure 8 shows three $V(x)$ curves computed for three different values of the normalized crack depth, $d/\lambda_{\mathrm{Ra}}$, of 0.1, 0.5 and 1.0 (where $\lambda_{\mathrm{Ra}}$ is the Rayleigh wavelength). It can be seen that the very shallow crack produces comparatively little contrast, because this crack neither reflects nor absorbs a significant proportion of the incident surface waves. On the other hand, the deeper cracks produce considerably more contrast, showing both long-range and short-range effects. The long-range Rayleigh ripple is more pronounced in the crack of intermediate depth because of the larger Rayleigh wave reflection coefficient; the short-range contrast is greatest in the deepest crack, which has the smallest transmission coefficient. To illustrate how

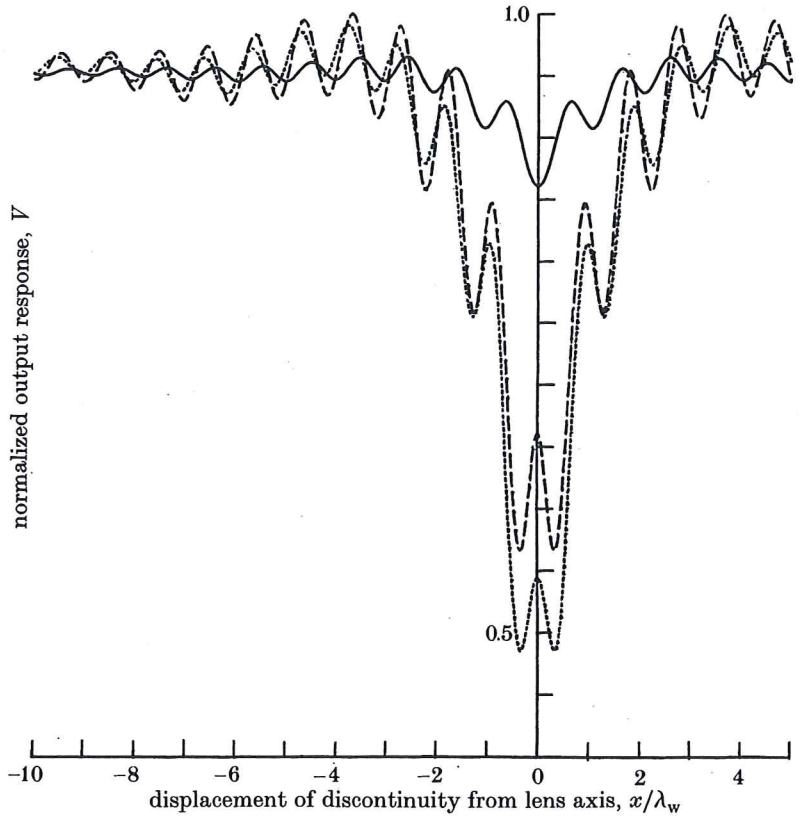


FIGURE 8. $V(x)$ curves calculated for the reflection and transmission coefficients obtained by Angel & Achenbach (1984). Because their results used the Poisson ratio 0.3 the relevant elastic properties were longitudinal velocity = 6000 m $s^{-1}$, shear velocity = 3207 m $s^{-1}$ and density 2695 kg $m^{-3}$. The corresponding Rayleigh wave velocity is 2974 m $s^{-1}$. Solid curve represents crack depth of $0.1\lambda_{Ra}$. Broken curve represents crack depth of $0.5\lambda_{Ra}$. Dotted curve represents crack depth of $\lambda_{Ra}$.

a typical discontinuity shows features characteristic of both types of idealized discontinuity, the dotted curve of figure 5 shows the same data as the solid curve of figure 8 but plotted on the same axes as the reflective and absorptive discontinuities.

In principle, therefore, it should be possible to use a cylindrical line focus lens to estimate the depth of cracks and an ability to sweep the acoustic frequency would greatly facilitate this.

### 5.2. *Results from a boundary between two different materials*

Equation (3.15) gives the scattering function for the general case when $k_{p1} \neq k_{p2}$; this enables us to calculate the $V(z)$ and $V(x)$ curves over a boundary between two media. The formulation enables one to calculate the scattering function for arbitrary values of reflection and transmission coefficients; however, the values used in our calculations correspond to those predicted by the transmission line equation (2.6). $V(z)$ curves for a boundary between two media whose acoustic

velocities differ are much more complicated than the single-media $V(z)$ curves. When the discontinuity is in the axis of the beam the periodicity observed is approximately intermediate between the periodicities of the individual media, as predicted by the simple ray theory of §2. When the position of the discontinuity is moved the curves become even more complicated, showing variations in periodicity as expected from the ray theory. The transitions in periodicity are, however, by no means as clear-cut as the ray theory predicts because diffraction effects are obviously important.

A series of $V(x)$ curves were calculated for a boundary between two media whose acoustic velocities differ by about 15 % (figure 9; the actual values are given in the caption). The $V(x)$ curves for different defocuses demonstrate many of the experimental findings in acoustic images. It should, however, be borne in mind that the two-dimensional lens modelled here may give greater amounts of contrast than are actually found with a spherical lens. Our model predicts that there is only a very small amount of long-range contrast in the form of periodic ripple in the $V(x)$

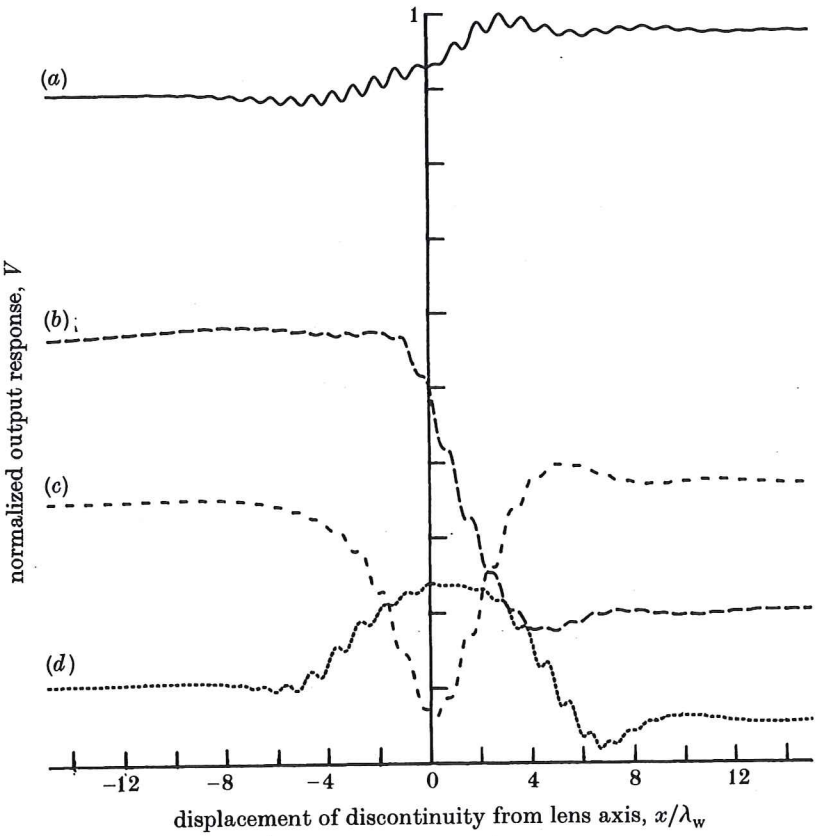


FIGURE 9. $V(x)$ calculated over two media with different elastic constants. Medium 1 is as aluminium above; medium 2 has the same density as medium 1 but the acoustic velocities are 5400 m s$^{-1}$ (longitudinal) and 2700 m s$^{-1}$ (shear). (*a*) Solid curve represents specimen at focus. (*b*) Long dashes represent a specimen defocus of $-4\lambda_w$. (*c*) Short dashes represent a specimen defocus of $-6\lambda_w$. (*d*) Dotted curve represents a specimen defocus of $-10\lambda_w$.

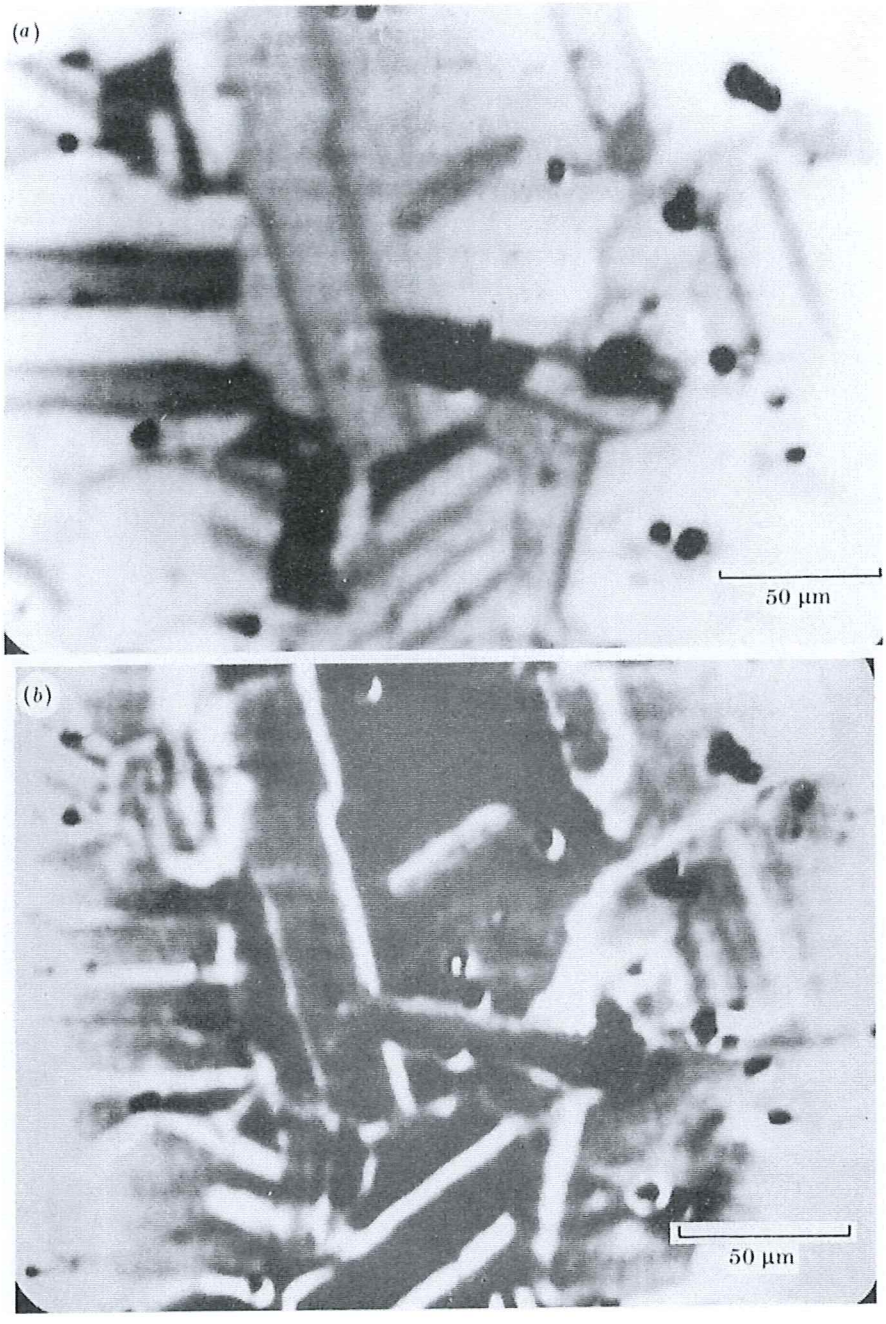


FIGURE 10. Acoustic micrographs of EN8 stainless steel showing grain boundary contrast (acoustic frequency 730 MHz). (*a*) Specimen defocus $-4$ μm ($\approx 2\lambda_w$). (*b*) Specimen defocus $-7$ μm ($\approx 3.5\lambda_w$).

(*Facing p.* 48)

curves. This is due to the small value of the Rayleigh wave reflection coefficient (*ca.* 0.07) expected from the transmission line model. In practice, one would expect there to be even less long-range contrast in a spherical imaging system, because the returning surface waves would only excite a very small proportion of the transducer. We are therefore able to understand the experimental observations that long-range Rayleigh wave ripple is rarely observed close to grain boundaries.

The most obvious difference between the $V(x)$ curves at an interface boundary and a crack is the lack of reflection symmetry about the interface position. As one moves away from the interface the output settles down to a level characteristic of the medium at that particular defocus. The curve, shown in figure 9*a* for a specimen at focus, shows a small amount of contrast between the two media and apart from the periodic ripple the transition across the interface is approximately monotonic, which suggests that the boundary would not show significant contrast on its own account. As the defocus is increased the transition between the two media initially remains approximately monotonic but the actual contrast between the two regions becomes greater. When the defocus is increased to $4\lambda_w$ (figure 9*b*), the relative contrast between the two regions is further increased and there is contrast reversal. The intensity at the position of the interface is more like the brightness level in medium 1 than medium 2; in an acoustic micrograph the grain boundary would thus appear to be displaced to the right. Figure 9*c* shows another feature often observed in acoustic micrographs. Here there is little contrast between the media but the boundary itself appears considerably darker than both regions. At a defocus of $10\lambda_w$ the contrast of the interface is reversed, so that the boundary appears very bright in comparison with the body of the two media (see figure 9*d*). The qualitative agreement with observation is striking because the most common sequence of images obtained in the s.a.m. correspond to that described above. That is to say, as one defocuses, acoustic images of grains appear before the boundary shows separate contrast. When the specimen is further defocused the boundary itself will stand out against the grains, almost invariably appearing dark. As the specimen is defocused still further the boundary will show up bright against the background of the grains. The acoustic images taken with a spherical lens bear this out. Figure 10*a*, plate 1, was taken at a defocus of $-4$ μm (*ca.* $2\lambda_w$) and shows dark grain boundaries. Figure 10*b* shows the grain boundaries appearing bright against the background; this image was taken at a defocus of $-7$ μm (*ca.* $3.5\lambda_w$). Although the values of defocus at which these light and dark boundaries appear are different in our two-dimensional model compared with the actual micrographs taken with a point-focus lens, the boundaries almost invariably show up dark at a smaller defocus than that at which they appear bright. It is also interesting that in the micrographs the contrast at the boundaries depends upon the defocus rather than the orientation of the individual grains making up the boundary, because the boundaries all appear light or dark within the same picture. It seems then that the transition from light to dark boundaries is a general feature of the amount of defocus rather than the specific grain discontinuities.

## 6. Discussion

Experimentally, the observation of contrast from linear discontinuities, including cracks, is very important as it is an area of application where the s.a.m. has very powerful imaging ability because the excited Rayleigh waves are scattered when they hit the crack broadside. In this paper we have presented a quantitative model which accounts for these phenomena for a cylindrical lens. The two-dimensional model explains many of the observed phenomena such as the different types of image which are observed in the acoustic microscope. The model also predicts that reflective discontinuities will give contrast in the region of positive defocus.

Probably one of the most important conclusions is the difference between the contrast mechanisms at linear discontinuities in a single medium and at interfaces between two media. Even though these two situations can be represented by the same general model, there is a significant difference in the physical interpretation of the contrast. In a crack in a single medium the output response of the microscope depends upon the scattering properties of the discontinuity, and a $V(x)$ trace must for obvious reasons be symmetrical about the position of the crack. On the other hand, there is no such symmetry at an interface boundary and so the image of the interface may appear slightly displaced from its true position. An even more important distinction between the two types of imaging is that a great deal of boundary contrast in the normal two-media situation (such as our two-dimensional approximation to a grain boundary) is not a result of the scattering properties of the interface but of the change in the wavenumber of the leaky Rayleigh wave. Although the transmission line model suggests that these two sets of properties are intimately linked, (3.15) allows the scattering properties of the interface to be separated from the elastic properties of the media, so that it is possible to calculate the $V(z)$ or $V(x)$ from a boundary with unity transmission coefficient and zero reflection coefficient. The $V(x)$ traces that one obtains are very similar to the $V(x)$ curves of figure 9 where the transmission line model for the scattering properties of the crack was used, the only significant difference being the absence of long-range ripple in the latter curves.

The practical consequences of this model are that the boundary conditions around lateral discontinuities, in a single medium, may be estimated from the observed contrast. It is expected to be much more difficult to use the s.a.m. for quantitative study of the boundary conditions at the boundary between two dissimilar materials, where the change in wavenumber across the interface is a strong additional contrast mechanism.

The model may fairly readily be extended to account for a single substrate with two discontinuities of variable separation, so that the lateral resolution of a two-dimensional lens which excites surface waves may be estimated. The theory presented here, although two-dimensional, should, in conjunction with experimental methods for measurement currently being developed, enable the scanning acoustic microscope to be exploited as a powerful instrument for quantitative study of surface features.

The authors thank the following for support: the SERC for a research fellowship for M.G.S.; the Royal Society and the Institute of Imaging Sciences of the Polytechnic Institute for a visiting fellowship for H.L.B. at University College, London; the Royal Society for a research fellowship for G.A.D.B. and the SERC and British Telecom Research Laboratories for funding N.J.B. We also thank Professor J. D. Achenbach for the provision of the phase information for the Rayleigh wave reflection and transmission coefficients omitted from the published version of his paper. Finally we thank Professor Sir Peter Hirsch, F.R.S., for support and encouragement during the course of this work.

## References

Achenbach, J. D., Gautesen, A. K. & Mendelsohn, D. A. 1980 *IEEE Trans.* **SU-27**, 124–129.

Atalar, A. 1979 *J. appl. Phys.* **50**, 8237–8239.

Angel, Y. C. & Achenbach, J. D. 1984 *J. acoust. Soc. Am.* **75**, 313–318.

Bertoni, H. L. 1984 *IEEE Trans.* **SU-31**, 105–116.

Bertoni, H. L. & Tamir, T. 1973 *Appl. Phys.* **2**, 157–172.

Cox, B. N. & Addison, R. S. 1984 Modelling the acoustic material signature in the presence of a surface-breaking crack. In *Review of quantitative non-destructive evaluation*, vol. 3B (ed. D. O. Thompson & D. E. Chimenti), pp. 1173–1184. Plenum Publishing Corporation.

Ilett, C., Somekh, M. G. & Briggs, G. A. D. 1984 *Proc. R. Soc. Lond.* A **393**, 171–183.

Li, R. C. M., Oliner, A. A. & Bertoni, H. L. 1977 *IEEE Trans.* **SU-24**, 66–78.

Parmon, W. & Bertoni, H. L. 1979 *Electron. Lett.* **15**, 684–686.

Quate, C. F. 1980 Microwaves, acoustics and scanning microscopy. In *Scanned image microscopy* (ed. E. A. Ash), pp. 23–55. London: Academic Press.

Quate, C. F., Atalar, A. & Wickramasinghe, H. K. 1979 *Proc. Instn. elect. Electron. Engrs* **67**, 1092–1114.

Saad, A., Bertoni, H. L. & Tamir, T. 1974 *Proc. Instn. elect. Electron. Engrs* **62**, 1552–1561.

Sheppard, C. J. R. & Wilson, T. 1981 *Appl. Phys. Lett.* **38**, 858–859.

Smith, I. R., Wickramasinghe, H. K., Farnell, G. W. & Jen, C. K. 1983 *Appl. Phys. Lett.* **42**, 411–413.

Somekh, M. G., Briggs, G. A. D. & Ilett, C. 1984 *Phil. Mag.* **49**A, 179–204.

Yamanaka, K. & Enomoto, Y. 1982 *J. appl. Phys.* **53**, 846–850.